Nonlinear State Estimation for QPSK Carrier Synchronization

Santiago Castillo

***Abstract*—This paper presents a nonlinear state estimation for carrier synchronization in a quadrature phase shift keying (QPSK) communication receiver. The synchronization problem is modeled as a discrete-time stochastic state estimation problem in which the carrier phase offset, frequency offset, frequency drift rate, and signal amplitude are treated as hidden states to be estimated from noisy in-phase and quadrature measurements. The Extended Kalman Filter (EKF) and Unscented Kalman Filter (UKF) are implemented and compared across multiple simulation scenarios. Results show that both estimators achieve effective carrier recovery, with comparable steady-state performance.**

I. Introduction

In a digital communication system, accurate demodulation requires the receiver to maintain synchronization with the incoming RF carrier. In practice, several physical effects distort the received signal and make this challenging.

One of the most prominent effects is carrier frequency offset (CFO) which occurs when the receiver's local oscillator is not perfectly synchronized with the transmitter's. This can occur due to oscillator inaccuracies or Doppler shifts. These frequency offsets accumulate over time and result in a rotating phase in the received baseband signal.

Additional distortions include signal amplitude variations due to channel fading and additive noise from receiver electronics.

Together, these distortions make accurate symbol detection difficult, and the receiver must estimate these carrier offsets in order to recover the transmitted symbol.

II. Methods

A. System Model

The system models a QPSK communication receiver operating with symbol period T. The transmitted baseband symbol at time index k is:

$$s_k \in \left\{ \frac{\pm 1 \pm j}{\sqrt{2}} \right\}$$

These four constellation points lie on the unit circle at $\pi/4$, $3\pi/4$, $5\pi/4$, and $7\pi/4$ radians. After downconversion and matched filtering, the received complex baseband signal is modeled as [1]:

$$r_k = a_k s_k e^{j\theta_k} + v_k$$

where θ_k is the carrier phase offset, a_k is the signal amplitude, and $v_k \sim \mathcal{CN}(0, \sigma^2)$ is complex AWGN. The complex exponential $e^{j\theta_k}$ acts as a rotation operator in the IQ plane, spinning the transmitted symbol by an unknown angle before it reaches the receiver. Separating into real and imaginary components:

$$\begin{aligned} \Re(r_k) &= a_k\big(\Re(s_k)\cos\theta_k - \Im(s_k)\sin\theta_k\big) + \Re(v_k) \\ \Im(r_k) &= a_k\big(\Re(s_k)\sin\theta_k + \Im(s_k)\cos\theta_k\big) + \Im(v_k) \end{aligned}$$

The dependence on $\cos(\theta_k)$ and $\sin(\theta_k)$ introduces the nonlinearity in the measurement model.

B. State-Space Formulation

The state vector to be estimated is:

$$x_k = \begin{bmatrix} \theta_k \\ \omega_k \\ \alpha_k \\ a_k \end{bmatrix}$$

The state equations are derived from the kinematic integrator relationships between phase, frequency, and drift [2], expanded to include the frequency drift state α_k:

$$\begin{aligned} \theta_{k+1} &= \theta_k + T\omega_k + \tfrac{T^2}{2}\alpha_k - Tu_k + n_{\theta,k} \\ \omega_{k+1} &= \omega_k + T\alpha_k - u_k + n_{\omega,k} \\ \alpha_{k+1} &= \alpha_k + n_{\alpha,k} \\ a_{k+1} &= a_k + n_{a,k} \end{aligned}$$

In matrix form:

$$x_{k+1} = \underbrace{\begin{bmatrix} 1 & T & \frac{T^2}{2} & 0 \\ 0 & 1 & T & 0 \\ 0 & 0 & 1 & 0 \\ 0 & 0 & 0 & 1 \end{bmatrix}}_{\Phi} x_k + \underbrace{\begin{bmatrix} -T \\ -1 \\ 0 \\ 0 \end{bmatrix}}_{\Gamma} u_k + n_k$$

The control input u_k is a frequency correction applied to the oscillator each symbol period. Because frequency integrates into phase over time, u_k appears in both the phase and frequency equations with gains of T and 1 respectively. All four eigenvalues of Φ are equal to one, showing that the open-loop system is marginally stable and provides no natural restoring force.

The measurement equation captures the IQ components of the received signal as a nonlinear function of the state:

$$y_k = \begin{bmatrix} y_{I,k} \\ y_{Q,k} \end{bmatrix} = h(x_k, s_k) + v_k$$

$$h(x_k, s_k) = \begin{bmatrix} a_k\big(\Re(s_k)\cos\theta_k - \Im(s_k)\sin\theta_k\big) \\ a_k\big(\Re(s_k)\sin\theta_k + \Im(s_k)\cos\theta_k\big) \end{bmatrix}$$

The transmitted symbol s_k is assumed known to the receiver via a pilot symbols.

C. Disturbance Modeling

All unknown disturbances are modeled as stochastic processes driven by i.i.d. random sequences, enabling the use of Kalman filtering techniques. The process noise vector $n_k \sim \mathcal{N}(0, Q)$ with:

$$Q = \mathrm{diag}(q_\theta,\ q_\omega,\ q_\alpha,\ q_a)$$

Each component drives a corresponding state as a first-order stochastic difference equation. The frequency drift α_k is the primary correlated disturbance in the system — it evolves as a random walk:

$$\alpha_{k+1} = \alpha_k + n_{\alpha,k}, \qquad n_{\alpha,k} \sim \mathcal{N}(0, q_\alpha)$$

This models the physical behavior of oscillator aging and temperature-induced frequency variation, where the drift rate changes slowly and continuously. By augmenting α_k into the state vector, the estimator jointly tracks the drift disturbance alongside the primary synchronization states, improving the prediction of both ω_k and θ_k over multiple steps. The measurement noise $v_k \sim \mathcal{N}(0, R)$ with $R = \sigma^2 I_2$ represents additive thermal noise from the receiver electronics, modeled as i.i.d. Gaussian.

D. Data Generation

The system was simulated in Simulink with all parameters listed in Table I. The open-loop plant took u_k and s_k as inputs and produced the true states x_k, measurements y_k, process noise n_k, and measurement noise v_k as outputs, all logged at each symbol period T.

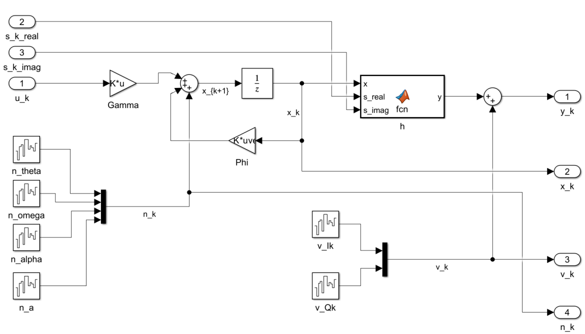

Fig. 1. Simulink Model of Open-Loop State Space

E. Extended Kalman Filter

The EKF linearizes the nonlinear measurement function h around the predicted state estimate using the Jacobian:

$$H_k = \left.\frac{\partial h}{\partial x}\right|_{\hat{x}_k^{(-)}}$$

Defining $A_k = \Re(s_k)\cos\hat{\theta}_k - \Im(s_k)\sin\hat{\theta}_k$ and $B_k = \Re(s_k)\sin\hat{\theta}_k + \Im(s_k)\cos\hat{\theta}_k$, we get the linearized matrix H:

TABLE I
SIMULATION PARAMETERS

Parameter	Symbol	Value	Units
Simulation Settings			
Number of symbols	N	500	–
Symbol period	T	1×10^{-4}	s
Initial True States			
Phase offset	θ_0	$\pi/3$	rad
Frequency offset	ω_0	$2\pi \times 200$	rad/s
Frequency drift	α_0	$2\pi \times 0.5$	rad/s^2
Amplitude	a_0	1.0	–
Process Noise Covariance			
Phase	q_θ	1×10^{-6}	rad^2
Frequency	q_ω	1×10^{-4}	(rad/s)^2
Drift	q_α	1×10^{-6}	(rad/s^2)^2
Amplitude	q_a	1×10^{-6}	–
Measurement Noise			
SNR	–	10	dB
Noise variance	σ^2	5×10^{-6}	–

$$H_k = \begin{bmatrix} -a_k B_k & 0 & 0 & A_k \\ a_k A_k & 0 & 0 & B_k \end{bmatrix}$$

The zero columns corresponding to ω_k and α_k demonstrate that these states are not directly observed, but estimated indirectly through the accumulated phase trajectory over time. The EKF update and prediction equations at each symbol period are:

$$\bar{K}_k = P_k^{(-)} H_k^T (H_k P_k^{(-)} H_k^T + R)^{-1} \tag{1}$$

$$\hat{x}_k^{(+)} = \hat{x}_k^{(-)} + \bar{K}_k (y_k - h(\hat{x}_k^{(-)}, s_k)) \tag{2}$$

$$P_k^{(+)} = (I - \bar{K}_k H_k) P_k^{(-)} \tag{3}$$

$$\hat{x}_{k+1}^{(-)} = \Phi\, \hat{x}_k^{(+)} + \Gamma\, u_k \tag{4}$$

$$P_{k+1}^{(-)} = \Phi\, P_k^{(+)}\, \Phi^T + Q \tag{5}$$

The estimator is initialized at $\hat{x}_0 = [0,\ 0,\ 0,\ a_{\text{nom}}]^T$ with initial covariance $P_0 = \mathrm{diag}[(\pi/2)^2,\ (2\pi \times 500)^2,\ (2\pi \times 5)^2,\ 0.25]$ which simulates the cold-start condition where no prior knowledge of phase or frequency offset is available.

F. Unscented Kalman Filter

Instead of computing a Jacobian, the UKF propagates a set of sample points through the nonlinear measurement function directly. These points are selected to exactly capture the mean and covariance of the prior state distribution.

III. RESULTS

A. Open-Loop Characterization

Before estimation, two open-loop scenarios were simulated to analyze the system behavior and justify the need for state estimation.

B. Zero-Synchronization Scenario

To establish a baseline, the system was first simulated with no synchronization applied, meaning $u_k = 0$ for all k. In this scenario, no correction is applied to the receiver oscillator.

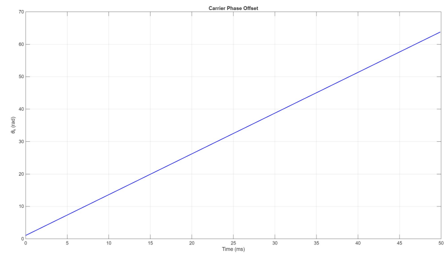

Fig. 2. Phase State Trajectory with $u_k = 0$

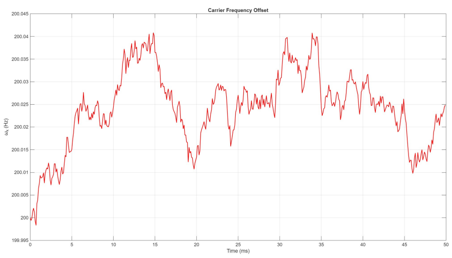

Fig. 3. Frequency State Trajectory with $u_k = 0$

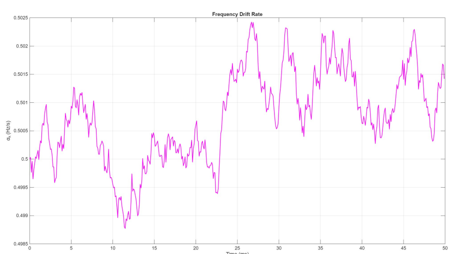

Fig. 4. Freq. Drift State Trajectory with $u_k = 0$

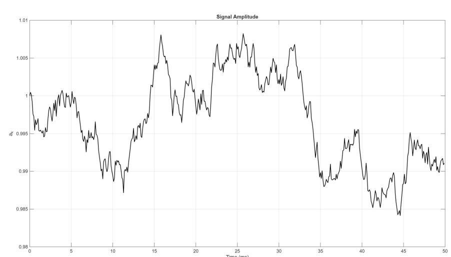

Fig. 5. Amplitude State Trajectory with $u_k = 0$

This allows the carrier phase and frequency offset evolve freely according to the model.

The resulting state trajectories are shown in the figures. The carrier phase θ_k accumulates linearly over time, which occurs due to the constant frequency offset of $\omega_0 = 200$ Hz. The total phase accumulation is roughly 20π radians which corresponds to approximately 10 full rotations of the constellation. The frequency offset ω_k and drift rate α_k remain close to their initial values which is expected given the small process noise variances. Lastly, the amplitude a_k varies slightly around its nominal value of 1.0 due to the random walk process noise.

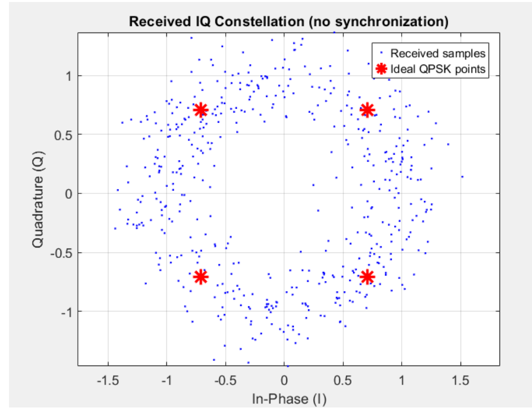

Fig. 6. Received QPSK Symbols with $u_k = 0$

The received constellation shown in Figure 6 depicts a ring of samples rather than clustering. This shape occurs because the CFO causes the constellation to rotate continuously, essentially "smearing" the samples uniformly around the unit circle. This behavior is expected when there is no synchronization since the receiver has no way of accounting for the phase rotation. Furthermore, the radial thickness of the ring reflects the amplitude variation in a_k over the simulation.

C. Ideal Unit-Impulse Synchronization Scenario

To show the effect of a perfect frequency correction, a unit-impulse input was applied at $k = 0$ with magnitude equal to the true frequency offset ω_0. It is important to note that this scenario is not physically realizable in practice, since it assumes perfect knowledge of the frequency offset at $k = 0$. However, it is useful to isolate the effect of the control input.

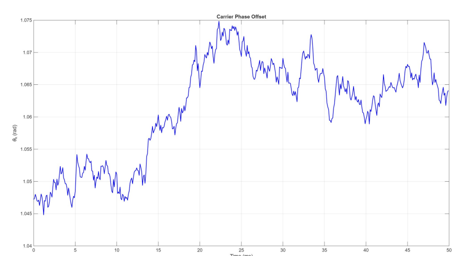

Fig. 7. Phase State Trajectory with $u_k = \omega_0 \cdot \delta[k]$

The resulting state trajectories are shown in the above figures. The effect of the frequency correction can be seen by the frequency offset ω_k settling near zero for the duration of the simulation. As a result, the carrier phase θ_k no longer accumulates linearly and instead remains close to its initial value of $\theta_0 = \pi/3$, with only a small slow drift of α_k.

However, the initial phase offset θ_0 is not corrected. This is because u_k has no direct effect on the existing phase offset θ_k in the state equations. The current open-loop system has no mechanism to remove it.

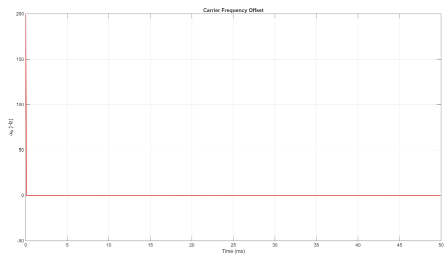

Fig. 8. Frequency State Trajectory with $u_k = \omega_0 \cdot \delta[k]$

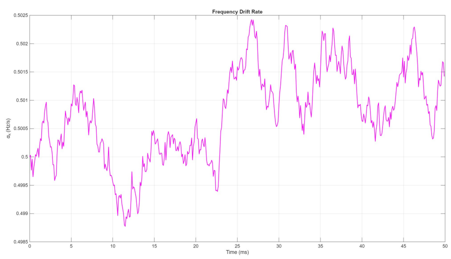

Fig. 9. Freq. Drift State Trajectory with $u_k = \omega_0 \cdot \delta[k]$

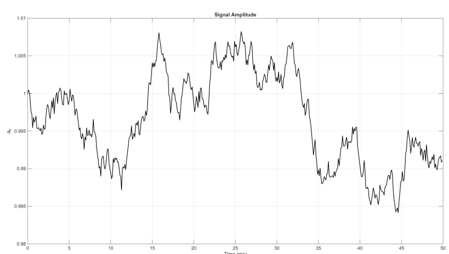

Fig. 10. Amplitude State Trajectory with $u_k = \omega_0 \cdot \delta[k]$

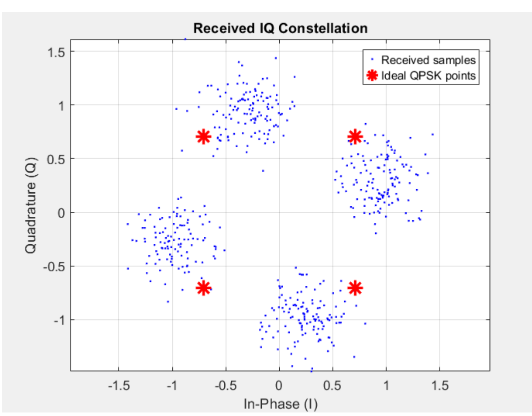

Fig. 11. Received QPSK Symbols with $u_k = \omega_0 \cdot \delta[k]$

The CFO correction can be seen in Figure 11. Instead of the constellation ring as when $u_k = 0$, the received samples now cluster around four distinct regions, essentially eliminating the smearing. However, the clusters are still phase shifted from the ideal QPSK constellation points by $\theta_0 = \pi/3$. This is a result of the uncompensated initial phase offset which demonstrates the limitation of frequency-only correction. Complete synchronization must estimate and compensate all 4 internal states, not just oscillator frequency. This then justifies the use of the Extended Kalman Filter for state estimation.

D. EKF Performance

Figures 12–15 show the EKF state estimates and estimation errors for the phase and amplitude states. The filter converges rapidly from the cold-start initial conditions, with the phase error settling within the 2σ bounds within the first 50 symbols.

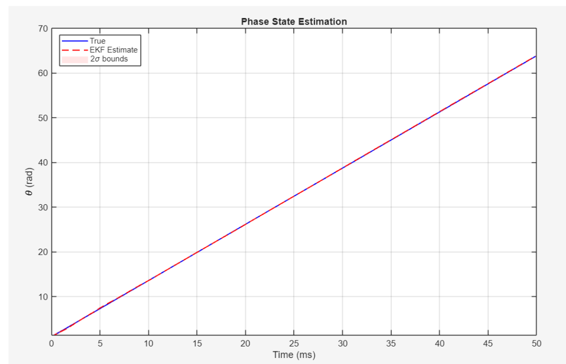

Fig. 12. EKF phase state estimate vs true state.

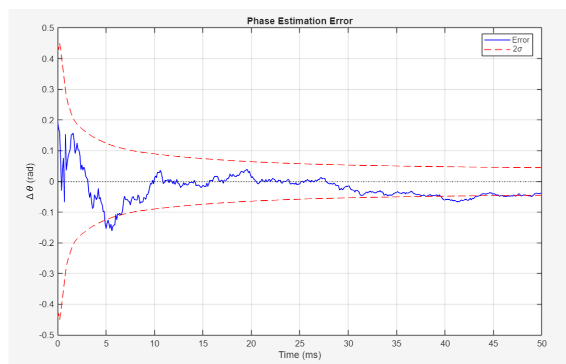

Fig. 13. EKF phase estimation error with 2σ bounds derived from P_k.

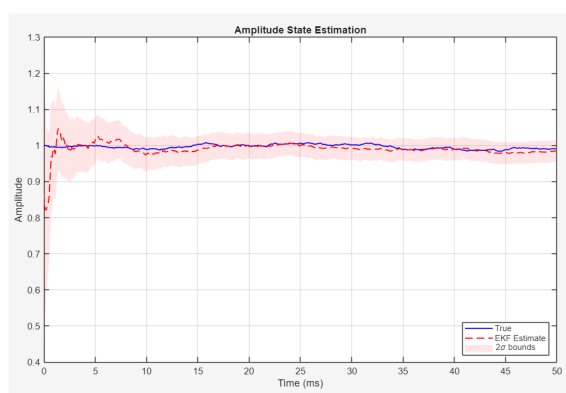

Fig. 14. EKF amplitude state estimate vs true state.

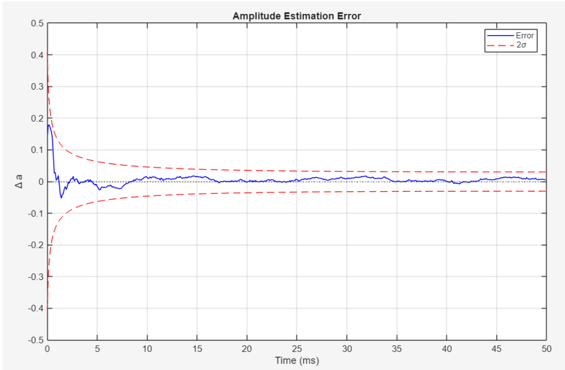

Fig. 15. EKF amplitude estimation error with 2σ bounds derived from P_k.

Fig. 16. IQ constellation after EKF correction. Tight clustering around ideal QPSK points confirms effective state estimation.

E. EKF vs UKF Comparison

Table II presents the RMSE comparison between the EKF and UKF across all four states.

TABLE II
ESTIMATION RMSE COMPARISON — EKF VS UKF

State	**EKF RMSE**	**UKF RMSE**
Phase offset θ_k (rad)	0.0501	0.0505
Frequency offset ω_k (Hz)	10.882	11.169
Frequency drift α_k (Hz/s)	0.6717	0.7105
Signal amplitude a_k	0.0207	0.0186

Figures 17 and 18 show the UKF estimation errors for the phase and amplitude states alongside the EKF for comparison.

The results show that the EKF and UKF perform comparably across all four states, with neither method having a clear advantage. The EKF achieves marginally lower RMSE for θ_k, ω_k, and α_k, while the UKF achieves a slightly lower RMSE for a_k. A better UKF performance would likely occur at a lower SNR, where the measurement noise is larger and the phase uncertainty at each step is greater, or during a cold start with a larger initial phase uncertainty.

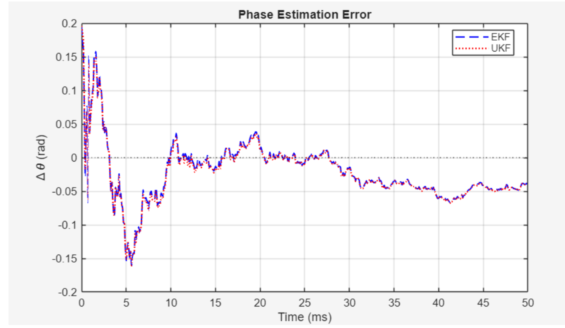

Fig. 17. Phase estimation error: EKF vs UKF.

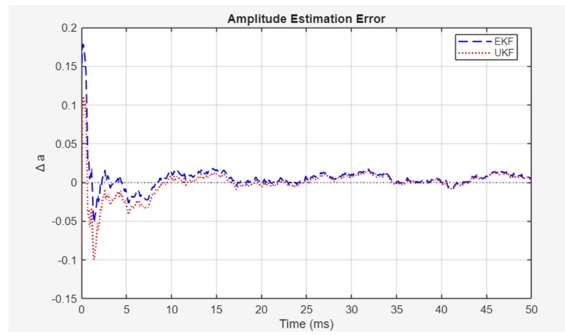

Fig. 18. Amplitude estimation error: EKF vs UKF.

IV. CONCLUSIONS

This paper presented a nonlinear state estimation framework for QPSK carrier synchronization, modeled as a discrete-time stochastic estimation problem with four hidden states. The EKF and UKF were implemented and evaluated on simulated data generated from a Simulink model of the open-loop receiver plant.

The open-loop simulations confirmed that uncompensated CFO causes continuous constellation rotation, and that frequency correction alone cannot remove an existing phase offset, justifying the need for the full four-state estimation. Both the EKF and UKF successfully recovered the carrier phase and amplitude, as evidenced by the corrected IQ constellation and the estimation errors remaining within the 2σ bounds derived from the state error covariance matrix. The two methods performed comparably at the nominal operating conditions of SNR = 10 dB, with the EKF offering a slight computational advantage.

For future work, to be able to correct a changing frequency offset in real time, the estimation loop could be closed by feeding $\hat{\omega}_k$ back to the oscillator as u_k would create a fully closed-loop digital PLL. This is much more realistic to how digital recievers correct CFO. Second, evaluating both estimators at lower SNR (0–5 dB) would stress-test the EKF linearization and would likely demonstrate a better performance for the UKF. Third, replacing the random walk amplitude model with a mean-reverting AR(1) process would be more realistic to how amplitude is affected in a wireless channel.

References

[1] L. Pakala and B. Schmauss, "Extended Kalman filtering for joint mitigation of phase and amplitude noise in coherent QAM systems," *Opt. Express*, vol. 24, pp. 6391–6401, 2016.

[2] T. Inoue and S. Namiki, "Carrier recovery for M-QAM signals based on a block estimation process with Kalman filter," *Opt. Express*, vol. 22, pp. 15376–15387, 2014.